Variable Angle Spectroscopic Ellipsometry investigation of CVD-grown monolayer graphene

Marco Castriota[1,3,5], Grazia Giuseppina Politano[1a], Carlo Vena[1], Maria Penelope De Santo[1,2], Giovanni Desiderio[2], Mariano Davoli[4], Enzo Cazzanelli[1,3,5], Carlo Versace[1,2]

1. *Dipartimento di Fisica, Università della Calabria 87036 Rende CS Italy*
2. *Licryl CNR/Nanotec c/o Dipartimento di Fisica, Università della Calabria 87036 Rende CS Italy*
3. *Consorzio Nazionale Interuniversitario per le Scienze Fisiche della Materia, Unità di Ricerca Cosenza*
4. *Dipartimento Biologia Ecologia e Scienze della Terra (DiB.E.ST.), Laboratorio Microscopia Elettronica, Ponte P. Bucci - Cubo 15A PT 87036 Rende CS Italy*
5. *Notredame s.r.l., c/o Dipartimento di Fisica, Università della Calabria, Italy*

Despite intensive investigations in the UV (ultraviolet) and visible range, the research on the optical properties of graphene in the extended near and mid infrared range by means of Spectroscopic Ellipsometry (SE) remains limited yet. Herein, the optical properties of a Chemical Vapor Deposition (CVD)-grown monolayer graphene, transferred from a copper substrate onto SiO_2/Si, were studied in the broad energy range (0.38-6.2 eV) using Variable Angle Spectroscopic Ellipsometry (VASE). The morphological and the structural properties of the samples were investigated by Micro-Raman Spectroscopy, Wavelength Dispersive X-ray (WDX) analysis, Scanning Electron Microscopy (SEM) and Atomic Force Microscopy (AFM). The Lorentz oscillator model proposed for the optical response of graphene fits very well the experimental data. An unintentional doping, revealed by Micro-Raman Spectroscopy and WDX, is reported.

Graphene; Optical constants, Spectroscopic ellipsometry; Doping; Raman Spectroscopy

[a] *Corresponding author* *E-mail address* : grazia.politano@unical.it (Grazia Giuseppina Politano)

1. Introduction

The study of the unique properties of graphene has been the main goal of several studies during the last years [1,2]. Graphene has revealed numerous unique physical and electrical properties [3,4]. In particular, its peculiar band structure and electron transport characteristics make it highly promising for a new generation of high-performance modulators, sources, and detectors operating across the infrared (IR) spectral region [5,6].

Several research groups have derived the complex refractive index of graphene by Spectroscopic Ellipsometry (SE), especially in the ultraviolet (UV) and visible range [7–9]. Nevertheless, very few works, (e.g., Chang et al [10]), concern SE characterization of chemical vapor deposited graphene in the extended near infrared and mid infrared range, because of the standard ellipsometry equipment limitations [11].

It is interesting to note that SE has been used to analyze the properties of graphene related materials [12,13] and their interaction with metals [14–16]. Furthermore, advances have been reported in the study of the transfer residue on the optical properties of chemical vapor deposited graphene investigated through SE [17,18].

The rise of the interest in graphene optical properties is shown in many recent ellipsometry studies: for example, graphene thin films have been studied from the point of view of depolarization effects [19] and the optical constants of graphene thin films have been determined from the Mueller matrix spectra [20].

The optical behavior of graphene differs significantly depending on the production technique, whether it has been exfoliated [21] or deposited through Chemical Vapor Deposition (CVD) [22]. CVD is a method which can make high quality graphene, potentially on a large scale [23].

In addition, the use of different substrates add an extra variable to make a proper comparison of optical graphene behavior, as reported in [24].

It has been shown that the silicon substrate covered by 300 nm of silicon oxide ensures a better graphene visibility, with an increasing of the contrast due to interference enhancement [25,26].

With respect to graphene device designs and performance enhancement, it is thus crucial to fully understand the optical properties of a monolayer graphene on SiO_2/Si obtained by CVD synthesis.

In the present study, broadband optical properties of the CVD grown graphene were measured by Variable Angle Spectroscopic Ellipsometry (VASE) in the photon energy range (between 0.38 and 6.2 eV).

In the range only little research has been reported, thus our work wants to fill this gap by means of an ellipsometer which combines high accuracy and precision with a wide spectral range.

Micro-Raman spectroscopy, Wavelength Dispersive X-ray (WDX), Scanning Electron Microscopy (SEM) and Atomic Force Microscopy (AFM) measurements were carried out on the graphene samples. It is worth noticing that Micro-Raman spectroscopy has been extensively used for studying carbon based materials such as carbon nanotubes and graphene [15,27–35].
Our findings open new avenues for graphene research, especially for applications in the intriguing IR range [36].

2. Experimental

Some commercially available samples of monolayer graphene on SiO_2/Si (doped P/Boron) bought from Graphenea Co. were investigated. Graphene was grown via CVD method. Then 18 μm thick copper foil was used as a catalyst and methane as carbon source. The graphene sheet was transferred by a polymethyl methacrylate (PMMA) assisted WET transfer process [37].
Micro-Raman spectra were collected using a Horiba-Jobin Yvon microprobe apparatus (spectral resolution ~2 cm^{-1}), equipped with a CCD (256x1024 pixels) detector cooled at -70 °C and with a 532 nm line of a diode laser, with an emitted power of 50 mW. A 50x Mplan Olympus objective was used, focusing a laser spot of about 2 μm of apparent diameter.
The Copper element distribution in the sample was analyzed by electron probe microanalysis (JXA-8230, EPMA) equipped with a WDX analysis. Standards-based WDX analyses were acquired for 30 seconds at 15 kV, with a 30 nA probe current and a 4 micron defocused beam diameter.
SEM analysis was accomplished with a FEI Quanta FEG 400 ESEM microscope.
Tapping mode AFM images were collected in ambient conditions with a Multimode 8 equipped with a Nanoscope V controller (Bruker Instruments). Images were acquired using cantilevers with a force constant k = 5 Nm^{-1} (model TAP150A, Bruker). The scan line speed was optimized between 1 and 3 Hz over 512 ×512 pixels. Image treatment and analysis were done using the free software WSxM [38].
The optical characterization of the sample has been performed by using VASE.
Spectra of the ellipsometric angles ψ and Δ were acquired using a V-VASE Ellipsometer (Woollam Co.) in the [0.38 -6.2] eV photon energy range.
The ellipsometric spectra were collected at 65°,70°,75° incident angles to improve the accuracy of layer modeling. The structural and morphological properties were estimated by using a multilayer optical model compatible with the ellipsometric experimental results. The optical model together with the best fitting values were calculated by WVASE32 [39] application using the nonlinear Levenberg-Marquardt algorithm [40]

3. Results and discussion

3.1 *Micro-Raman Spectroscopy and WDX measurements*

Raman spectroscopy is used to characterize the quality of the transferred graphene samples.

The optical microscopy investigations show that in the samples there are zones with different colors: dark (zone A) mostly at the center of the samples, slightly clearer (zone B) near the border of the samples, and, finally, clear stripes distributed in the samples as defects (zone C) (Fig. 1).

The Raman investigations were performed on many points of all the zones. The results show that the graphene is predominantly monolayer, with bilayer and multilayer patches at many of its nucleation sites, which are evident in the "Morphological SEM and AFM section". These few –layer graphene patches can be attributed to the carbon segregation and are typical of CVD graphene on polycrystalline Cu [41–43].

In Fig.1, two representative micrographs are reported: in Fig. 1(a), representing a central zone of the sample, darker regions are labeled as A while the brighter stripe is labeled as C; in Fig. 1(b), representing a border region of the sample, the homogeneous region is labeled as B.

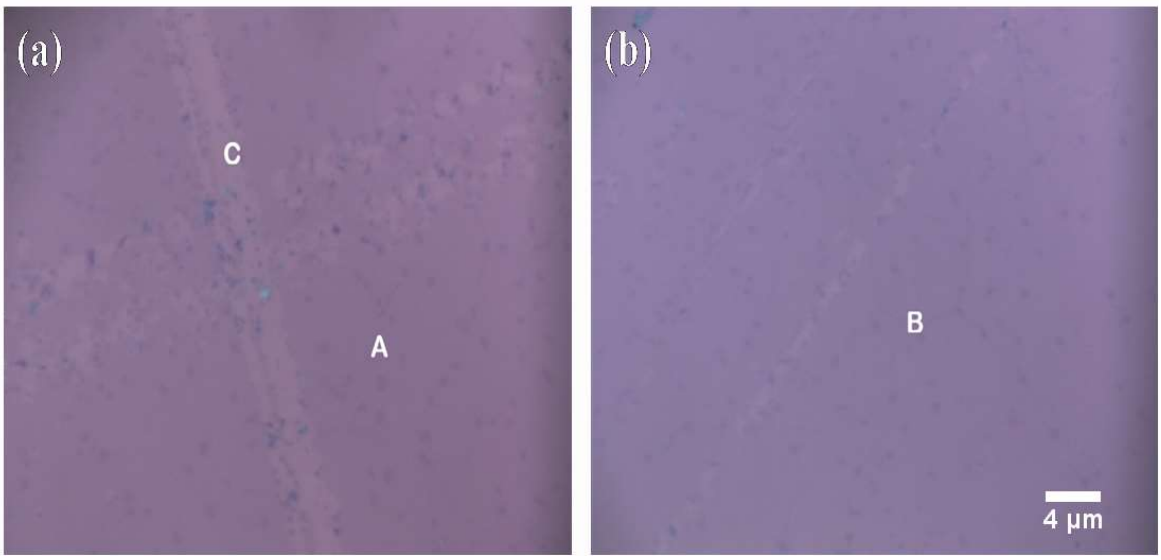

Fig. 1: Region near the center of the sample, where a darker zone (A zone in the text) and a brighter stripe (C zone in the text) are visible (a), homogeneous region near the border of the sample (B zone in the text) (b).

Raman spectra have been collected in all cases for wavenumbers above 400 cm^{-1} to observe both the Si substrate Raman modes, (the first order optical phonon of Si and the other broad band around 960 cm^{-1} due to 2TO overtone [44]), and the ones of the transferred graphene films. Only the latter, relevant to the present study, are shown in the figures while the Si modes can be useful as standards.

In Fig. 2 representative Raman spectra collected on the zone A in the wavenumber range between 400 cm^{-1} and 1100 cm^{-1} (a) and between 1200 cm^{-1} and 3400 cm^{-1} (b) are reported.

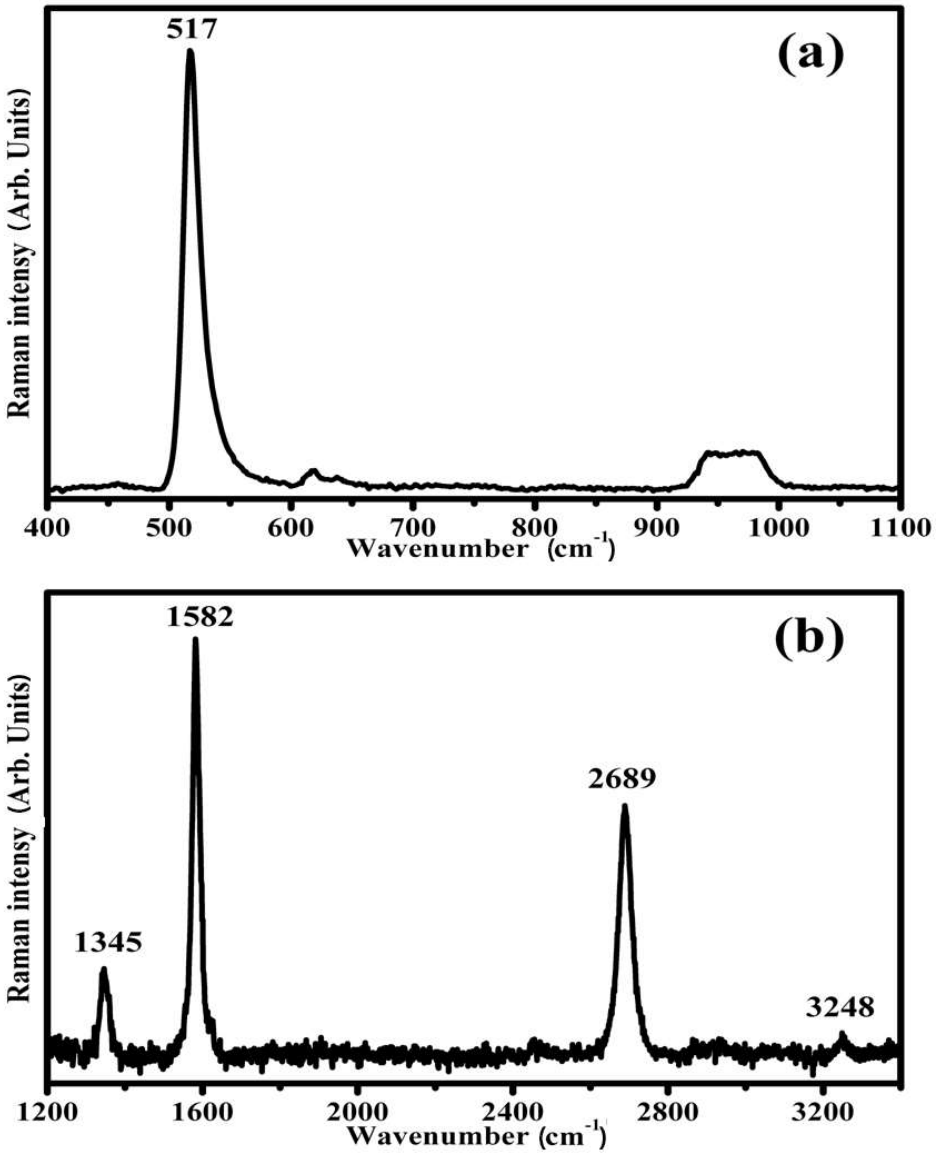

Fig. 2: Representative Raman spectra collected on the central zone (Fig.1 zone A) of the Graphene/Si samples. Raman spectra between 400 cm^{-1} and 1100 cm^{-1} (a) and 1200 cm^{-1} and 3400 cm^{-1}(b).

As it can be seen, the main Raman features fall at 1345, 1582, 2689 and 3248 cm^{-1}. The small band at 1345 cm^{-1} is assigned to graphene D band, the band at 1582 cm^{-1} is the G band and the bands at 2689 cm^{-1} and 3248 cm^{-1} are the overtones 2D and 2D' [15,28,30,33].

In Fig. 3 representative Raman spectra collected on the zone B in the wavenumber range between 400 cm^{-1} and 1100 cm^{-1} (a) and between 1200 cm^{-1} and 3400 cm^{-1} (b) are reported.

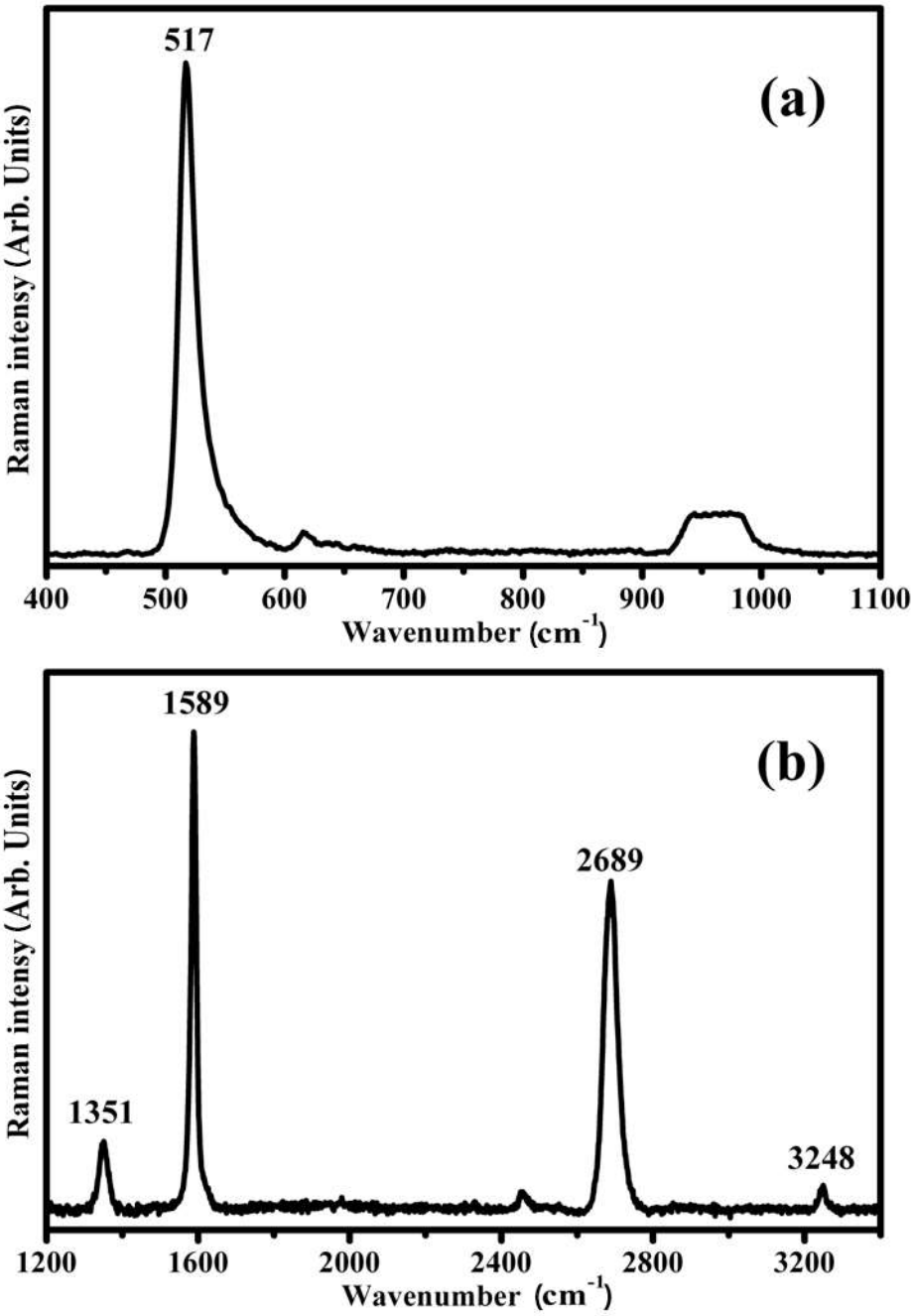

Fig.3: Representative Raman spectra collected on the border zone (Fig.1 zone B) of the Graphene/Si samples. Raman spectra between 400 cm^{-1} and 1100 cm^{-1} (a) and 1200 cm^{-1} and 3400 cm^{-1} (b).

It is possible to see that the D (1351 cm^{-1}) band and the G (1589 cm^{-1}) band are slightly blue shifted while the 2D (2689 cm^{-1}) band and 2D' (3248 cm^{-1}) band fall at the same frequency of the spectra shown in Fig. 2. In the spectrum of zone B, it is also possible to observe the presence of the band at 2454 cm^{-1}, designed as D''+D', where D'' falls at about 1073cm^{-1} [45].

In Fig. 4 representative Raman spectra collected on the zone C in the wavenumber range between 400 cm^{-1} and 1100 cm^{-1} (a) and between 1200 cm^{-1} and 3400 cm^{-1} (b) are reported.

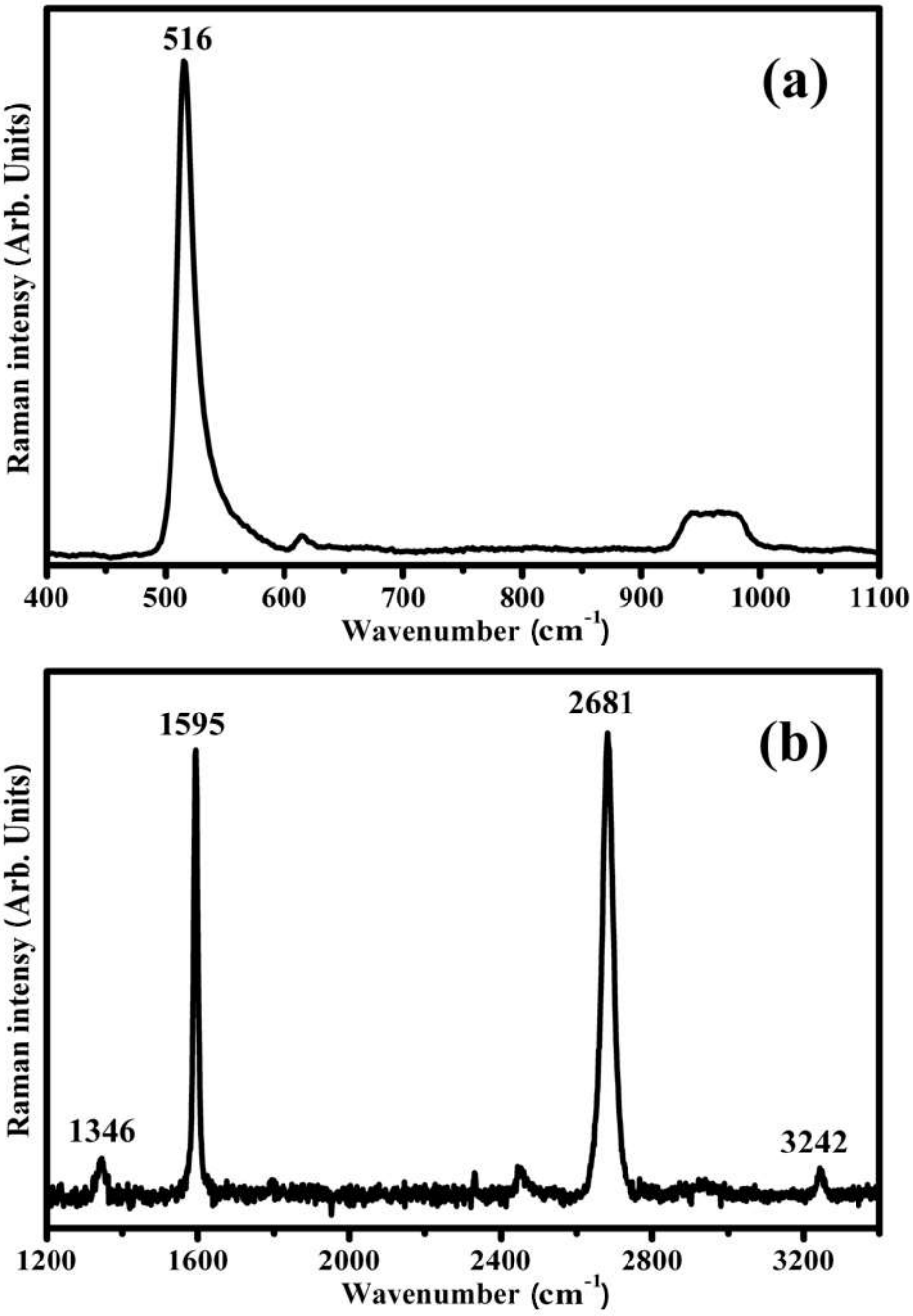

Fig. 4: Representative Raman spectra collected on defects of the layer (Fig.1 zone C) of the Graphene/Si samples. Raman spectra between 400 cm^{-1} and 1100 cm^{-1} (a) and 1200 cm^{-1} and 3400 cm^{-1} (b).

In this last case, only the G band (1595 cm^{-1}) is remarkably blue shifted while the other bands are all down shifted: D band at 1346 cm^{-1}, 2D band at 2681 cm^{-1} and 2D' band at 3242 cm^{-1}. Also in the last spectra the band D''+D' is detected.

The intensity ratio between the 2D band and the G band is indicative of the numbers of the graphene layers [30,44,45]: if I_{2D}/I_G value is higher than 2, then it indicates the presence of monolayer graphene;

if I_{2D}/I_G value is in the range between 1 and 2, then it indicates the formation of bilayer graphene; if I_{2D}/I_G value is lower than 1, then it indicates the presence of three or more layers [30].
In Table I the main characteristics of the Lorentzian functions used for fitting the bands D, G and 2D of the Raman spectra in Figs. 2,3,4 are reported.

	D BAND			G BAND			2D BAND			I_D/I_G	I_{2D}/I_G
Zone	*Raman shift (cm^{-1})*	*FWHM (cm^{-1})*	*A*	*Raman shift (cm^{-1})*	*FWHM (cm^{-1})*	*A*	*Raman shift (cm^{-1})*	*FWHM (cm^{-1})*	*A*		
A	1347	22	4611	1583	20.27	20142	2690	35	21039	0.23	1.044
B	1350	23	8981	1589	14.70	39295	2688	35	66206	0.23	1.68
C	1345	20	2296	1595	11.40	17655	2681	29	46492	0.13	2.63

Table I: Raman shifts, Full Width at Half Maximum (FWHM) and intensities *A* of the D, G and 2D bands and relative intensity ratios, obtained by using Lorentzian function in the fitting procedure for three representative sample zones.

In the A (Fig.2) and B (Fig.3) zones of the analyzed samples the I_{2D}/I_G ratio values are 1.04 and 1.68 respectively. In the C zone (Fig.4) the I_{2D}/I_G ratio value is 2.63. It means that, even though the graphene is predominantly monolayer, there are some areas in the central and border zones where there are bilayer graphene patches, while monolayer graphene is found in the most bright stripes[30,44–46]. The study of the Full Width at Half Maximum (FWHM) obtained for the G bands in the Raman spectra of the three regions confirms such results. In fact, the FWHM of the G band of the spectra of the zone A is 20.27 cm^{-1} and it is quite wide and due to thicker graphene film, while the FWHM of the G band of the spectra of the zone C is 11.4 cm^{-1}, quite sharp and ascribed to the presence of a single graphene layer. The FWHM of the G band of the spectra in region B (14.7 cm^{-1}) is due to a graphene multilayer deposition thinner than that of region A.
These first conclusions made on the basis of Raman band intensity ratio are clearly confirmed by the visual inspection of the optical microscopy images, which reveal different color for different thickness of graphene deposited layer, as observed in many previous studies of graphene on Si, for instance Castriota et al. [28]
As previously outlined in the experimental section, these samples are first obtained on copper foils and lately transferred on Si/SiO_2 substrate by a PMMA assisted wet transfer process.
The different values obtained for the G band (1583 cm^{-1} for the A zone , 1589 cm^{-1} for the B zone and 1595 cm^{-1} for the C zone) in the different zones of the sample can be explained in terms of hole doping and compressive strain[30,47]. Therefore, it is possible to state that doping effects as well as

stress can play some role during the transfer, and such effects can change the Raman features [30,48,49]. The small shift of the 2D band seen above can be explained taking in account the results obtained by I_{2D}/I_G ratio. In fact, the 2D band falls at 2689 cm^{-1} in the case of bilayer graphene and at 2681 cm^{-1} in the case of the monolayer graphene. Lastly, with regard to the D band, the increased value (1351cm^{-1}) shown in the spectra collected on the border region, with those collected on the central zone (1345 cm^{-1}) and on the defected region (1346 cm^{-1}), could be assigned to the compression induced by the edge of the graphene layer [28,30].

By using WDX analysis traces of copper (0.015±0.001)% were detected.

3.2 Morphological SEM and AFM analysis

The CVD-grown graphene film shows some defects in terms of small holes, cracks, folding and wrinkles.

Fig. 5(a) and related magnification Fig. 5(b) reveal the growth of fractures and domain borders.

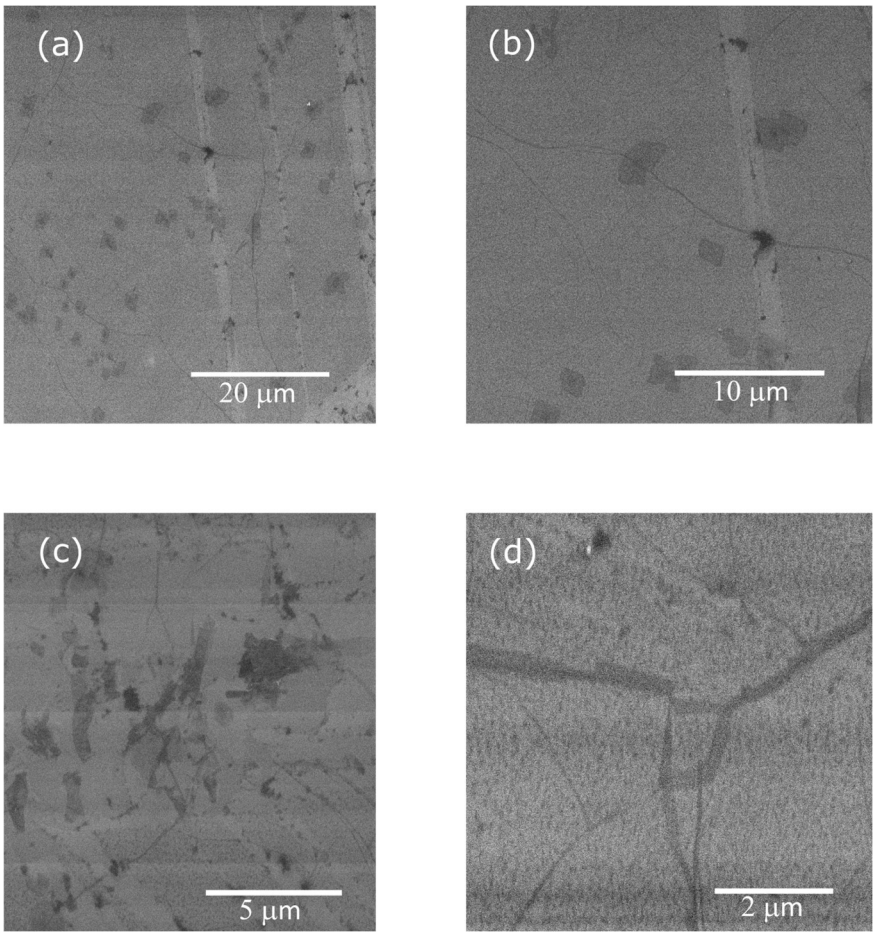

Fig. 5: Scanning electron microscope (SEM) detector images of the graphene layer grown on copper substrate and transferred to SiO_2/Si substrate. Graphene domains and wrinkles are clearly visible (a) and related magnification (b). Folding lines and small holes appear (c) and related magnification (d).

In particular, it is possible to see a single layer of graphene with some patches of different thickness (domain borders). CVD-grown graphene is known to be polycrystalline [50]. During the CVD growth, multiple nucleation events take place on the copper substrate to produce graphene patches that finally unite together to make a continuous film [51]. Evidence of the presence of patches of multilayer graphene was shown in the Raman measurements, reported in the previous section. The size of each crystalline domain varies from several hundred nanometers to several microns.

The wrinkles (see Fig. 5(a) and Fig. 5(b)) are formed during the growth and transfer of graphene. CVD growth of graphene is carried out at 1000° C on a copper substrate. At the same time as graphene is cooled to room temperature (the last step of CVD growth), wrinkles appear in the graphene film because of the great difference in the thermal expansion coefficients between the graphene and the underlying substrate [51]. Moreover, the rough copper substrate contributes to the formation of wrinkles upon the transfer of graphene to the silicon wafer [52]. In the wrinkled areas the graphene may be folded (Fig. 5(c) and related magnification Fig. 5(d)). In Fig. 5(c) it can be seen that the domain borders areas predominately nucleate at the wrinkles suggesting that these areas could be nucleation sites for growth [53]. Small holes are visible in Fig. 5(d).

Fig.6 shows a 1μm x1μm AFM image of the sample.

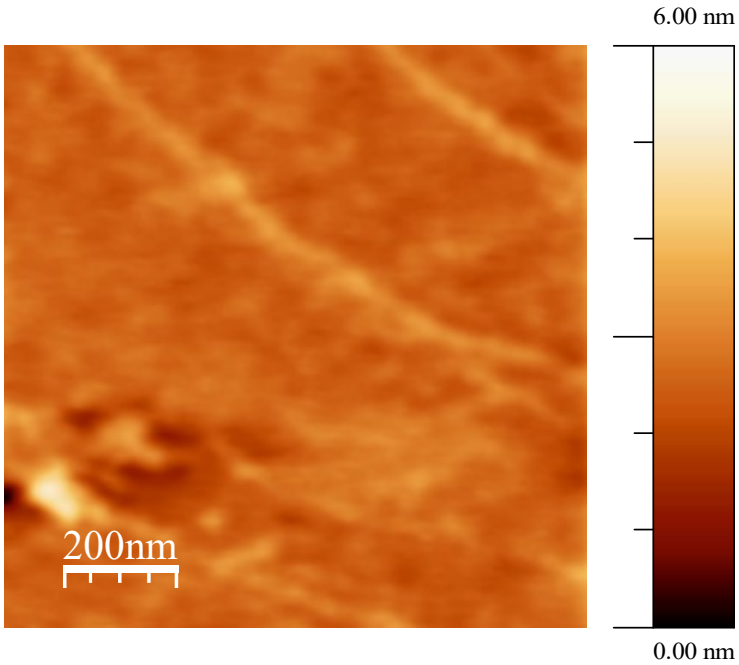

Fig. 6: Atomic Force Microscopy (AFM) image of a CVD-grown single layer graphene transferred on a silicon wafer.

The surface of graphene is dominated by micron-sized wrinkles that are 2–6 nm in height, which are caused by the transfer of graphene, as observed in the SEM images. The roughness analysis from the AFM showed that the Root Mean Square (RMS) roughness is around 0.3 nm.

3.3 Variable Angle Spectroscopic Ellipsometry measurements

The system was modeled as follows (see Table II for a scheme of the optical model).

3	**Graphene**	0.345 nm
2	**EMA interlayer**	5.4 nm
1	**SiO_2**	287 nm
0	**Si**	1 mm

Table II: Scheme of the optical model of monolayer graphene on silicon substrate.

Bottom to top, the Si substrate and the SiO_2 film (287 nm) were introduced, an Effective Medium Approximation (EMA) layer (5.4 nm) was added as a spacer between graphene and the substrate to account for the presence of some molecules of water resulting from the transfer process [24,54], and finally the monolayer graphene (0.345 nm) was considered.
The graphene thickness was considered a constant value (reported in the specification sheet of the sample) and thus left out of the interpolating fitting procedure.
Weber et al [11] have reported the problems of depolarization with ordinary ellipsometry equipment in the studies of graphene thin films .In our measurements the depolarization factor was always less than 10%.
The graphene monolayer was modeled as the sum of four Lorentz oscillators to keep consistency with the Kramers-Kronig relations [55].The complex dielectric function is described by the relation:

$$\tilde{\varepsilon}(hv) = \varepsilon_1 + i\varepsilon_2 = \varepsilon_\infty + \sum_{k=1}^{N} \frac{A_k}{{E_k}^2 - E^2 - i\Gamma_k E} \qquad (1)$$

where E is the energy of the incident photons, $\varepsilon_\infty$is the real part of the dielectric function when $E \to \infty$, A_k is the strength expressed in eV^2, Γ_k is the broadening in eV end E_k is the central energy of the k-th oscillator. A_k also indicates the percentage contribution of oscillator k to the whole system.
Table III shows the parameters obtained from the best fit with a low Mean Squared Error (MSE).

$d(\mathrm{nm})$	0.345 ± 0.010
ε_∞	$3.7\ \pm0.2$
$A_1(eV^2)$	30.6 ± 0.1
$\Gamma_1(eV)$	$0.82\pm0.\ 01$
$E_1(eV)$	4.51 ± 0.01
$A_2(eV^2)$	78.9 ± 0.1
$\Gamma_2(eV)$	$6.6\pm0.\ 2$
$E_2(eV)$	$2.82\ \pm0.01$
$A_3(eV^2)$	25.2 ± 0.3
$\Gamma_3(eV)$	$4.1\ \pm0.2$
$E_3(eV)$	2.36 ± 0.01
$A_4(eV^2)$	5.0 ± 0.1
$\Gamma_4(eV)$	$0.08\ \pm0.01$
$E_4(eV)$	0.51 ± 0.02

Table III: Lorentz oscillators parameters resulting from the best fit of ellipsometric experimental data for the CVD monolayer graphene sample. Amplitude A_k has unit of eV^2 while center energy E_k and broadening Γ_k have units of eV; d is the thickness of film in nm ; the high-frequency dielectric constant dielectric constant ε_∞ is dimensionless.

In Fig. 7(a) and Fig. 7(b) the generated and experimental data of the ψ and Δ spectra are reported for different angles of incidence in the [0.38 -6.2] eV photon energy range for the CVD monolayer graphene.

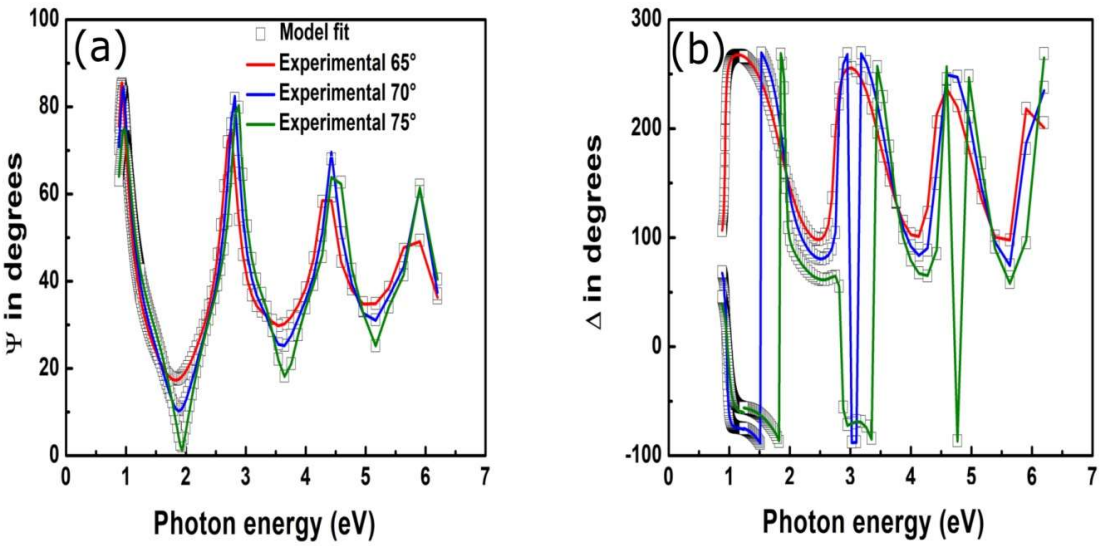

Fig. 7: Variable Angle Spectroscopic Ellipsometry (VASE) measurements of graphene on silicon substrate. Experimental and model generated ψ (a) and Δ (b) data fits at different angles of incidence.

Fig. 8 shows the dispersion laws estimated by ellipsometry characterization.

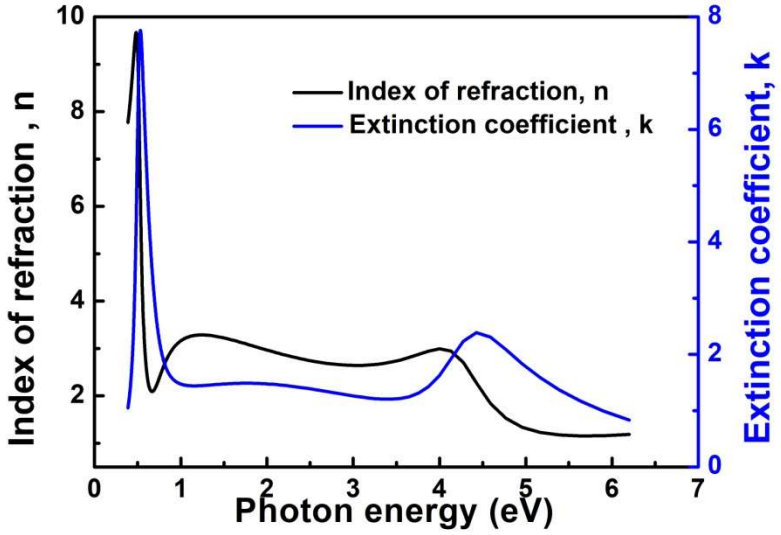

Fig.8: Estimated dispersion laws of the monolayer graphene by ellipsometry characterization. The curves represent the index of refraction (black lines) and the extinction coefficient (blue lines).

The position of the maximum in the extinction coefficient (4.5 eV, k=2.4) is similar to values obtained by Nelson et al. [8].The peak is due to a van Hove singularity in the density of states, which is close to the hopping energy *t* [56] .

The absorption peak at 4.5 eV is, thus, due to the effects of resonant excitons on the interband transition peak that would occur at 5.1 eV in the independent particle picture [57].Comparing our results with those reported by other groups [24], some differences in the maximum of the extinction coefficient may arise, taking into consideration that the excitonic response at the van Hove singularity is dependent on the competition between electron–electron and electron–hole interactions [58]. Therefore, the differences on the substrate characteristics could produce variations in the position and symmetry of the UV extinction peak.

Furthermore, it must be taken into account that structural imperfections (grain boundaries, defects, residues from transfer, bilayer and multilayer graphene patches etc.) exist in CVD grown graphene, as we had reported in the "Micro-Raman Spectroscopy and WDX measurements" and in the "Morphological SEM and AFM analysis" sections, which could cause some variations in the optical constants. The oscillator at 2.36 eV can be related to the resonant excitonic effects due to the electron –hole interaction in the π and π^* at the M point [57], while the oscillator at ~ 2.8 eV can be attributable to the hopping amplitude *t* giving rise to the Dirac nature of low lying excitations [59].

As it can be seen in Fig.8, the optical absorption of graphene in the visible and near-infrared regime is constant.

The fitting ellipsometric model seems also to indicate the formation of a conducting layer with Drude-like electrons, with a main contribution to the absorption found at 0.5 eV, as shown in Table III.

The optical properties of graphene arise from its unique band structure and 2D nature. Depending on the wavelength regime, two distinct contributions need to be considered [60].While interband transitions define the optical response from visible down to near -infrared photon energies, intraband processes corresponding to conduction by free carriers become important in the long-wavelength region [61,62].

It is possible that our CVD graphene was unintentionally doped during the synthesis. Previous studies have shown that a wide range of sources can contribute to such unintentional doping, including residual metallic contamination [63,64], the SiO_2 substrate [65], H_2O [26], and PMMA [66] residues. In the sections "Micro-Raman Spectroscopy and WDX measurements" it is shown that the CVD –grown graphene sample contains traces of copper by using WDX analysis. In

addition, doping effects can play some role during the wet transfer process, as revealed by Micro-Raman Spectroscopy.

The doping concentration of our sample was estimated from the optical conductivity data, as described in the **Supplementary material**. The extracted value is $n \approx 7.8 \times 10^{13}\, cm^{-2}$. For unintentional residual and surface adsorbate doping, the carrier density is normally at the scale of 10^{11}–10^{12} cm^{-2} [67]. Nevertheless, the work by Nistor *et al* [68] suggests that SiO_2 defects can act as a reservoir for graphene's charge carriers, contributing up to $n \approx 9.6 \times 10^{13}\, cm^{-2}$ p-type carriers.

4. Conclusions

The broad band (0.38 eV-6.2 eV) optical properties of a commercial monolayer CVD- grown graphene were studied by means of Variable Angle Spectroscopic Ellipsometry. The graphene sheet was grown on copper and then transferred on Si/SiO_2 substrate by a PMMA assisted WET transfer process.

The morphological and the structural properties of the samples were investigated by Micro-Raman Spectroscopy, WDX, SEM and AFM measurements.

The monolayer graphene was modeled as the sum of four Lorentz oscillators. The absorption peak at 4.5 eV is due to the effects of resonant excitons on the interband transition peak. The oscillator at 2.36 eV can be related to the resonant excitonic effects due to the electron –hole interaction in the π and π^* at the M point, while the oscillator at ~ 2.8 eV can be attributable to the hopping amplitude t giving rise to the Dirac nature of low lying excitations. The fitting ellipsometric model indicates also the formation of a conducting layer with Drude-like electrons, with a main contribution to the absorption found at 0.5 eV.

Micro–Raman characterization revealed that in our sample there are doping effects, probably due to some impurities introduced during the transfer. In particular, traces of copper $(0.015 \pm 0.001)\%$ were revealed by using WDX analysis. The estimated carrier density from optical conductivity data is $n \approx 7.8 \times 10^{13}\, cm^{-2}$.

Visual inspection of optical micrograph and the related micro-Raman measurements show that in the graphene transferred films there is the presence of monolayer regions and bilayer ones, may be even three layers, in different zones. In addition, the CVD-grown graphene film has some defects in terms of small holes, cracks, folding and wrinkles, as it can be seen in the SEM images. These structural imperfections could cause some variations in the optical constants.

The present study will serve as a reference in the graphene optical framework and in designing electronic and optoelectronic devices for advanced applications in a broadband optical range, especially in the IR range.

ACKNOWLEDGEMENTS

This work was partially supported by POR CALABRIA FESR-FSE 2014-2020 -ASSE I – PROMOZIONE DELLA RICERCA E DELL'INNOVAZIONE Obiettivo specifico 1.2 Azione 1.2.2" Project: "MERAVIGLIE".
The authors are grateful to Dr. Federica Ciuchi for useful discussions.

[1] M.J. Allen, V.C. Tung, R.B. Kaner, Honeycomb Carbon: A Review of Graphene, Chem. Rev. 110 (2010) 132–145. doi:10.1021/cr900070d.

[2] L.A. Falkovsky, Optical properties of graphene, J. Phys. Conf. Ser. 129 (2008) 12004. http://stacks.iop.org/1742-6596/129/i=1/a=012004.

[3] S. Das Sarma, S. Adam, E.H. Hwang, E. Rossi, Electronic transport in two-dimensional graphene, Rev. Mod. Phys. 83 (2011) 407–470. https://link.aps.org/doi/10.1103/RevModPhys.83.407.

[4] R.R. Nair, P. Blake, A.N. Grigorenko, K.S. Novoselov, T.J. Booth, T. Stauber, N.M.R. Peres, A.K. Geim, Fine Structure Constant Defines Visual Transparency of Graphene, Science (80-.). 320 (2008) 1308 LP-1308. http://science.sciencemag.org/content/320/5881/1308.abstract.

[5] A. Tredicucci, M.S. Vitiello, Device Concepts for Graphene-Based Terahertz Photonics, IEEE J. Sel. Top. Quantum Electron. 20 (2014) 130–138. doi:10.1109/JSTQE.2013.2271692.

[6] F. Bonaccorso, Z. Sun, T. Hasan, A.C. Ferrari, Graphene photonics and optoelectronics, Nat. Photonics. 4 (2010) 611. http://dx.doi.org/10.1038/nphoton.2010.186.

[7] J.W. Weber, V.E. Calado, M.C.M. van de Sanden, Optical constants of graphene measured by spectroscopic ellipsometry, Appl. Phys. Lett. 97 (2010) 91904. doi:10.1063/1.3475393.

[8] F.J. Nelson, V.K. Kamineni, T. Zhang, E.S. Comfort, J.U. Lee, A.C. Diebold, Optical properties of large-area polycrystalline chemical vapor deposited graphene by spectroscopic ellipsometry, Appl. Phys. Lett. 97 (2010) 253110. doi:10.1063/1.3525940.

[9] W. Li, G. Cheng, Y. Liang, B. Tian, X. Liang, L. Peng, A.R. Hight Walker, D.J. Gundlach, N. V Nguyen, Broadband optical properties of graphene by spectroscopic ellipsometry, Carbon N. Y. 99 (2016) 348–353. doi:https://doi.org/10.1016/j.carbon.2015.12.007.

[10] Y.-C. Chang, C.-H. Liu, C.-H. Liu, Z. Zhong, T.B. Norris, Extracting the complex optical conductivity of mono- and bilayer graphene by ellipsometry, Appl. Phys. Lett. 104 (2014) 261909. doi:10.1063/1.4887364.

[11] J.W. Weber, K. Hinrichs, M. Gensch, M.C.M. van de Sanden, T.W.H. Oates, Microfocus infrared ellipsometry characterization of air-exposed graphene flakes, Appl. Phys. Lett. 99 (2011) 61909. doi:10.1063/1.3624826.

[12] S. Funke, U. Wurstbauer, B. Miller, A. Matković, A. Green, A. Diebold, C. Röling, P.H.

Thiesen, Spectroscopic imaging ellipsometry for automated search of flakes of mono- and n-layers of 2D-materials, Appl. Surf. Sci. 421 (2017) 435–439. doi:https://doi.org/10.1016/j.apsusc.2016.10.158.

[13] S. Schöche, N. Hong, M. Khorasaninejad, A. Ambrosio, E. Orabona, P. Maddalena, F. Capasso, Optical properties of graphene oxide and reduced graphene oxide determined by spectroscopic ellipsometry, (2017). doi:https://doi.org/10.1016/j.apsusc.2017.01.035.

[14] G.G. Politano, C. Vena, G. Desiderio, C. Versace, Spectroscopic ellipsometry investigation of the optical properties of graphene oxide dip-coated on magnetron sputtered gold thin films, J. Appl. Phys. 123 (2018) 55303. doi:10.1063/1.5007430.

[15] G.G. Politano, E. Cazzanelli, C. Versace, C. Vena, M.P. De Santo, M. Castriota, F. Ciuchi, R. Bartolino, Graphene oxide on magnetron sputtered silver thin films for SERS and metamaterial applications, Appl. Surf. Sci. Volume 427 (2018) 927–933. doi:https://doi.org/10.1016/j.apsusc.2017.09.059.

[16] A.M. Kostruba, Influence of the graphene substrate on morphology of the gold thin film. Spectroscopic ellipsometry study, Appl. Surf. Sci. 283 (2013) 603–611. doi:https://doi.org/10.1016/j.apsusc.2013.06.156.

[17] A. Kasikov, T. Kahro, L. Matisen, M. Kodu, A. Tarre, H. Seemen, H. Alles, The optical properties of transferred graphene and the dielectrics grown on it obtained by ellipsometry, Appl. Surf. Sci. 437 (2018) 410–417. doi:https://doi.org/10.1016/j.apsusc.2017.08.109.

[18] A. Matković, U. Ralević, M. Chhikara, M.M. Jakovljević, D. Jovanović, G. Bratina, R. Gajić, Influence of transfer residue on the optical properties of chemical vapor deposited graphene investigated through spectroscopic ellipsometry, J. Appl. Phys. 114 (2013) 93505. doi:10.1063/1.4819967.

[19] Z. Pápa, J. Csontos, T. Smausz, Z. Toth, J. Budai, Spectroscopic ellipsometric investigation of graphene and thin carbon films from the point of view of depolarization effects, Appl. Surf. Sci. 421 (2017) 714–721. doi:https://doi.org/10.1016/j.apsusc.2016.11.231.

[20] B. Song, H. Gu, S. Zhu, H. Jiang, X. Chen, C. Zhang, S. Liu, Broadband optical properties of graphene and HOPG investigated by spectroscopic Mueller matrix ellipsometry, Appl. Surf. Sci. (2018). doi:https://doi.org/10.1016/j.apsusc.2018.01.051.

[21] V.G. Kravets, A.N. Grigorenko, R.R. Nair, P. Blake, S. Anissimova, K.S. Novoselov, A.K. Geim, Spectroscopic ellipsometry of graphene and an exciton-shifted van Hove peak in absorption, Phys. Rev. B. 81 (2010) 155413. http://link.aps.org/doi/10.1103/PhysRevB.81.155413.

[22] M. Losurdo, M.M. Giangregorio, P. Capezzuto, G. Bruno, Ellipsometry as a Real-Time Optical Tool for Monitoring and Understanding Graphene Growth on Metals, J. Phys. Chem. C. 115 (2011) 21804–21812. doi:10.1021/jp2068914.

[23] Y. Zhang, L. Zhang, C. Zhou, Review of Chemical Vapor Deposition of Graphene and Related Applications, Acc. Chem. Res. 46 (2013) 2329–2339. doi:10.1021/ar300203n.

[24] E. Ochoa-Martinez, M. Gabas, L. Barrutia, A. Pesquera, A. Centeno, S. Palanco, A. Zurutuza, C. Algora, Determination of a refractive index and an extinction coefficient of standard production of CVD-graphene, Nanoscale. 7 (2015) 1491–1500. doi:10.1039/C4NR06119E.

[25] P. Blake, E.W. Hill, A.H. Castro Neto, K.S. Novoselov, D. Jiang, R. Yang, T.J. Booth, A.K. Geim, Making graphene visible, Appl. Phys. Lett. 91 (2007) 63124. doi:10.1063/1.2768624.

[26] K.S. Novoselov, A.K. Geim, S. V Morozov, D. Jiang, Y. Zhang, S. V Dubonos, I. V Grigorieva, A.A. Firsov, Electric Field Effect in Atomically Thin Carbon Films, Science (80-.). 306 (2004) 666 LP-669. http://science.sciencemag.org/content/306/5696/666.abstract.

[27] E. Cazzanelli, M. Castriota, L.S. Caputi, A. Cupolillo, C. Giallombardo, L. Papagno, High-temperature evolution of linear carbon chains inside multiwalled nanotubes, Phys. Rev. B. 75 (2007) 121405. https://link.aps.org/doi/10.1103/PhysRevB.75.121405.

[28] M. Castriota, E. Cazzanelli, D. Pacilè, L. Papagno, Ç.O. Girit, J.C. Meyer, A. Zettl, M. Giarola, G. Mariotto, Spatial dependence of Raman frequencies in ordered and disordered monolayer graphene, Diam. Relat. Mater. 19 (2010) 608–613. doi:https://doi.org/10.1016/j.diamond.2009.12.013.

[29] C. A., C. M., C. E., C. L., G. C., M. G., P. L., Second-order Raman scattering from linear carbon chains inside multiwalled carbon nanotubes, J. Raman Spectrosc. 39 (2008) 147–152. doi:10.1002/jrs.1871.

[30] C. Enzo, D.L. Oreste, V. Danilo, P. Alfonso, C. Marco, D. Giovanni, D.S.M. Penelope, A. Alfredo, F. Angela, R. Tania, A.R. Giuseppe, Characterization of graphene grown on copper foil by chemical vapor deposition (CVD) at ambient pressure conditions, J. Raman Spectrosc. 0 (2018). doi:10.1002/jrs.5375.

[31] E. Cazzanelli, M. Castriota, G. Mariotto, J.M. Rosolen, Microraman Study of Single Wall Carbn Nanotubes Obtained by Arc Method Using Metal and Oxide Catalysts, Surf. Eng. 19 (2003) 454–460. doi:10.1179/026708403225010163.

[32] A.P. and T.C. and R.G.A. and E.M. and G.C. and E.C. and V.F. and M.C. and E. Cazzanelli, Electronic, chemical and structural characterization of CNTs grown by SiC surface decomposition, J. Phys. Conf. Ser. 100 (2008) 52093. http://stacks.iop.org/1742-6596/100/i=5/a=052093.

[33] G.G. Politano, C. Versace, C. Vena, M. Castriota, F. Ciuchi, A. Fasanella, G. Desiderio, E. Cazzanelli, Physical investigation of electrophoretically deposited graphene oxide and reduced graphene oxide thin films, J. Appl. Phys. 120 (2016) 195307. doi:10.1063/1.4968000.

[34] M. Castriota, E. Cazzanelli, L. Caputi, A. Cupolillo, C. Giallombardo, L. Papagno, G. Mariotto, Investigations on Raman bands from carbon linear chains in multiwalled carbon nanotubes, Diam. Relat. Mater. 17 (2008) 1716–1723. doi:https://doi.org/10.1016/j.diamond.2008.01.019.

[35] E. Cazzanelli, L. Caputi, M. Castriota, A. Cupolillo, C. Giallombardo, L. Papagno, Carbon linear chains inside multiwalled nanotubes, Surf. Sci. 601 (2007) 3926–3932. doi:https://doi.org/10.1016/j.susc.2007.04.153.

[36] F.J. García de Abajo, Graphene Plasmonics: Challenges and Opportunities, ACS Photonics. 1 (2014) 135–152. doi:10.1021/ph400147y.

[37] J.W. Suk, A. Kitt, C.W. Magnuson, Y. Hao, S. Ahmed, J. An, A.K. Swan, B.B. Goldberg, R.S. Ruoff, Transfer of CVD-Grown Monolayer Graphene onto Arbitrary Substrates, ACS Nano. 5 (2011) 6916–6924. doi:10.1021/nn201207c.

[38] WSXM: A software for scanning probe microscopy and a tool for nanotechnology, Rev. Sci. Instrum. 78 (2007) 13705. doi:10.1063/1.2432410.

[39] I. J. A. Woollam Co., WVASE manual "Guide to Using WVASE32," 2010.

[40] J.J. Moré, The Levenberg-Marquardt algorithm: Implementation and theory, in: G.A. Watson (Ed.), Numer. Anal. Proc. Bienn. Conf. Held Dundee, June 28--July 1, 1977, Springer Berlin Heidelberg, Berlin, Heidelberg, 1978: pp. 105–116. doi:10.1007/BFb0067700.

[41] Z. Han, A. Kimouche, A. Allain, H. Arjmandi-Tash, A. Reserbat-plantey, S. Pairis, V. Reita, N. Bendiab, J. Coraux, V. Bouchiat, Suppression of Multilayer Graphene Patches during CVD Graphene growth on Copper, 2012.

[42] A.W. Robertson, J.H. Warner, Hexagonal Single Crystal Domains of Few-Layer Graphene on Copper Foils, Nano Lett. 11 (2011) 1182–1189. doi:10.1021/nl104142k.

[43] K. Yan, H. Peng, Y. Zhou, H. Li, Z. Liu, Formation of Bilayer Bernal Graphene: Layer-by-Layer Epitaxy via Chemical Vapor Deposition, Nano Lett. 11 (2011) 1106–1110. doi:10.1021/nl104000b.

[44] B. Li, D. Yu, S.-L. Zhang, Raman spectral study of silicon nanowires, Phys. Rev. B. 59 (1999) 1645–1648. https://link.aps.org/doi/10.1103/PhysRevB.59.1645.

[45] P. Tan, L. An, L. Liu, Z. Guo, R. Czerw, D.L. Carroll, P.M. Ajayan, N. Zhang, H. Guo, Probing the phonon dispersion relations of graphite from the double-resonance process of Stokes and anti-Stokes Raman scatterings in multiwalled carbon nanotubes, Phys. Rev. B. 66 (2002) 245410. https://link.aps.org/doi/10.1103/PhysRevB.66.245410.

[46] L. Liu, H. Zhou, R. Cheng, Y. Chen, Y.-C. Lin, Y. Qu, J. Bai, I.A. Ivanov, G. Liu, Y. Huang, X. Duan, A systematic study of atmospheric pressure chemical vapor deposition growth of large-area monolayer graphene, J. Mater. Chem. 22 (2012) 1498–1503. doi:10.1039/C1JM14272K.

[47] A.C. Ferrari, Raman spectroscopy of graphene and graphite: Disorder, electron–phonon coupling, doping and nonadiabatic effects, Solid State Commun. 143 (2007) 47–57. doi:https://doi.org/10.1016/j.ssc.2007.03.052.

[48] W. Choi, M.A. Shehzad, S. Park, Y. Seo, Influence of removing PMMA residues on surface of CVD graphene using a contact-mode atomic force microscope, RSC Adv. 7 (2017) 6943–6949. doi:10.1039/C6RA27436F.

[49] H. Van Ngoc, Y. Qian, S.K. Han, D.J. Kang, PMMA-Etching-Free Transfer of Wafer-scale Chemical Vapor Deposition Two-dimensional Atomic Crystal by a Water Soluble Polyvinyl Alcohol Polymer Method, Sci. Rep. 6 (2016) 33096. http://dx.doi.org/10.1038/srep33096.

[50] A. Kumari, N. Prasad, P.K. Bhatnagar, P.C. Mathur, A.K. Yadav, C. V Tomy, C.S. Bhatia, Electrical transport properties of polycrystalline CVD graphene on SiO2/Si substrate, Diam. Relat. Mater. 45 (2014) 28–33. doi:https://doi.org/10.1016/j.diamond.2014.03.003.

[51] S.Z. and S.P.S. and Z.L. and H. Liu, Photochemical oxidation of CVD-grown single layer graphene, Nanotechnology. 23 (2012) 355703. http://stacks.iop.org/0957-4484/23/i=35/a=355703.

[52] S. Deng, V. Berry, Wrinkled, rippled and crumpled graphene: an overview of formation mechanism, electronic properties, and applications, Mater. Today. 19 (2016) 197–212.

doi:https://doi.org/10.1016/j.mattod.2015.10.002.

[53] R.W. and R.P. and J.G. and T.P. and F.Z. and A.P. and N.K. and R.J. and A.Z. and L. Hao, Investigation of CVD graphene topography and surface electrical properties, Surf. Topogr. Metrol. Prop. 4 (2016) 25001. http://stacks.iop.org/2051-672X/4/i=2/a=025001.

[54] M. Magnozzi, N. Haghighian, V. Miseikis, O. Cavalleri, C. Coletti, F. Bisio, M. Canepa, Fast detection of water nanopockets underneath wet-transferred graphene, Carbon N. Y. 118 (2017) 208–214. doi:https://doi.org/10.1016/j.carbon.2017.03.022.

[55] R. Kubo, M. Ichimura, Kramers-Kronig Relations and Sum Rules, J. Math. Phys. 13 (1972) 1454–1461. doi:10.1063/1.1665862.

[56] A.H. Castro Neto, F. Guinea, N.M.R. Peres, K.S. Novoselov, A.K. Geim, The electronic properties of graphene, Rev. Mod. Phys. 81 (2009) 109–162. https://link.aps.org/doi/10.1103/RevModPhys.81.109.

[57] L. Yang, J. Deslippe, C.-H. Park, M.L. Cohen, S.G. Louie, Excitonic Effects on the Optical Response of Graphene and Bilayer Graphene, Phys. Rev. Lett. 103 (2009) 186802. https://link.aps.org/doi/10.1103/PhysRevLett.103.186802.

[58] K.F. Mak, J. Shan, T.F. Heinz, Seeing Many-Body Effects in Single- and Few-Layer Graphene: Observation of Two-Dimensional Saddle-Point Excitons, Phys. Rev. Lett. 106 (2011) 46401. https://link.aps.org/doi/10.1103/PhysRevLett.106.046401.

[59] H. Hadipour, S. Jafari, The importance of electron correlation in graphene and hydrogenated graphene, 2015. doi:10.1140/epjb/e2015-60454-1.

[60] L.M.M. and K.F.M. and A.H.C.N. and N.M.R.P. and T.F. Heinz, Observation of intra- and inter-band transitions in the transient optical response of graphene, New J. Phys. 15 (2013) 15009. http://stacks.iop.org/1367-2630/15/i=1/a=015009.

[61] N.M.R. Peres, Colloquium: The transport properties of graphene: An introduction, Rev. Mod. Phys. 82 (2010) 2673–2700. https://link.aps.org/doi/10.1103/RevModPhys.82.2673.

[62] V.P. Gusynin, S.G. Sharapov, J.P. Carbotte, Unusual Microwave Response of Dirac Quasiparticles in Graphene, Phys. Rev. Lett. 96 (2006) 256802. https://link.aps.org/doi/10.1103/PhysRevLett.96.256802.

[63] X. Liang, B.A. Sperling, I. Calizo, G. Cheng, C.A. Hacker, Q. Zhang, Y. Obeng, K. Yan, H. Peng, Q. Li, X. Zhu, H. Yuan, A.R. Hight Walker, Z. Liu, L. Peng, C.A. Richter, Toward Clean and Crackless Transfer of Graphene, ACS Nano. 5 (2011) 9144–9153. doi:10.1021/nn203377t.

[64] G. Lupina, J. Kitzmann, I. Costina, M. Lukosius, C. Wenger, A. Wolff, S. Vaziri, M. Östling, I. Pasternak, A. Krajewska, W. Strupinski, S. Kataria, A. Gahoi, M.C. Lemme, G. Ruhl, G. Zoth, O. Luxenhofer, W. Mehr, Residual Metallic Contamination of Transferred Chemical Vapor Deposited Graphene, ACS Nano. 9 (2015) 4776–4785. doi:10.1021/acsnano.5b01261.

[65] Y. Shi, X. Dong, P. Chen, J. Wang, L.-J. Li, Effective doping of single-layer graphene from underlying ${\text{SiO}}_{2}$ substrates, Phys. Rev. B. 79 (2009) 115402. https://link.aps.org/doi/10.1103/PhysRevB.79.115402.

[66] A. Pirkle, J. Chan, A. Venugopal, D. Hinojos, C.W. Magnuson, S. McDonnell, L. Colombo, E.M. Vogel, R.S. Ruoff, R.M. Wallace, The effect of chemical residues on the physical and

electrical properties of chemical vapor deposited graphene transferred to SiO2, Appl. Phys. Lett. 99 (2011) 122108. doi:10.1063/1.3643444.

[67] S. Goniszewski, M. Adabi, O. Shaforost, S.M. Hanham, L. Hao, N. Klein, Correlation of p-doping in CVD Graphene with Substrate Surface Charges, Sci. Rep. 6 (2016) 22858. http://dx.doi.org/10.1038/srep22858.

[68] R.A. Nistor, M.A. Kuroda, A.A. Maarouf, G.J. Martyna, Doping of adsorbed graphene from defects and impurities in SiO${}_{2}$ substrates, Phys. Rev. B. 86 (2012) 41409. doi:10.1103/PhysRevB.86.041409.

Supplementary material

Extraction of carrier density

The complex optical conductivity $\sigma = \sigma_1 + \sigma_2$ is related to the complex dielectric constant $\varepsilon = \varepsilon_1 + \varepsilon_2$

by the following relations [1]:

$\sigma_1 = \varpi \varepsilon_2 \varepsilon_0$ and $\sigma_2 = \varpi \varepsilon_1 \varepsilon_0$ (1)

where ϖ is the angular frequency, ε_0 is the free space dielectric constant.

The carrier density can be determined from the energy $2E_f$ at which the Pauli blocking occurs [2]. This energy can be found from the minimum in the imaginary part of the optical conductivity σ_2, from the frequency where the derivative of σ_2 with respect to frequency is zero [3].

Note that E_F (Fermi energy) of Dirac fermions scales with the 2D carrier density as n:

$$E_f = \hbar v_f \sqrt{\pi |n|} \qquad (2)$$

where v_f is the Fermi velocity and n is the carrier density. For the value of the Fermi velocity, the numeric value of $v_f \approx 1.0 \times 10^6 \frac{m}{s}$ is assumed [2].

It is thus possible to obtain the carrier concentration using Equation (2):

$$n = \frac{\left(\frac{E_f}{\hbar v_f} \right)^2}{\pi} \qquad (3)$$

In Fig. S1 it is reported the plot of the derivative of σ_2 with respect to frequency.

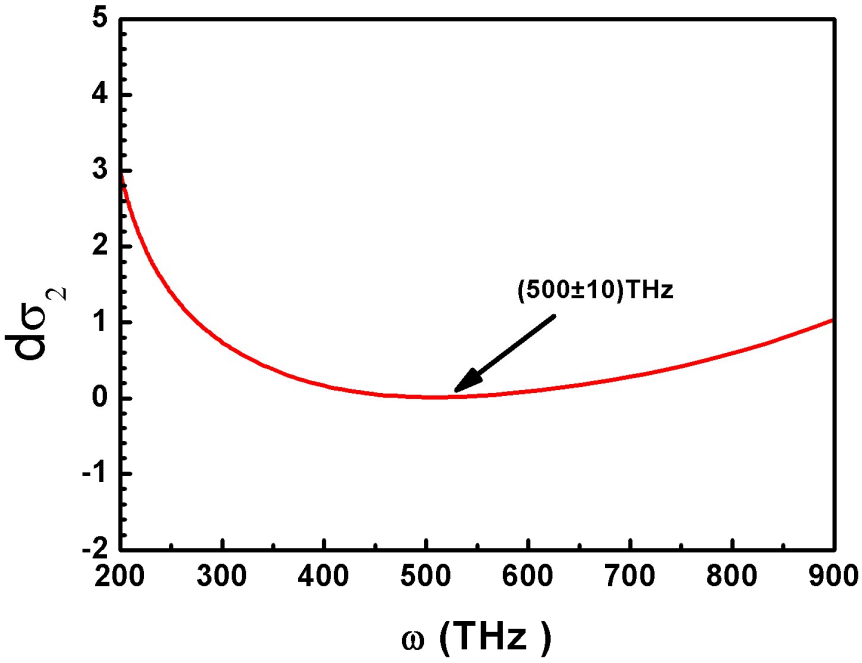

Fig. S1: plot of the derivative of the imaginary part σ_2 with respect to frequency.

We have found that the derivative is 0 at $\varpi = \frac{2E_f}{h} = 500THz$ .Using equation (3), the estimated carrier density is $n = (7.8 \pm 0.3) \times 10^{13} cm^{-2}$.

Alternatively, $2E_f$ values can be extracted from the center frequency of the $2E_f$ threshold in σ_1, real part of the optical conductivity. However ,the second method has larger errors, due to the uncertainty of defining the center of the $2E_f$ threshold, as reported by Li et al [3].

[1] F. Yakuphanoglu, M. Sekerci, O.F. Ozturk, The determination of the optical constants of Cu(II) compound having 1-chloro-2,3-o-cyclohexylidinepropane thin film, Opt. Commun. 239 (2004) 275–280. doi:https://doi.org/10.1016/j.optcom.2004.05.038.

[2] J.W. Weber, A.A. Bol, M.C.M. van de Sanden, An improved thin film approximation to accurately determine the optical conductivity of graphene from infrared transmittance, Appl. Phys. Lett. 105 (2014) 13105. doi:10.1063/1.4889852.

[3] Z.Q. Li, E.A. Henriksen, Z. Jiang, Z. Hao, M.C. Martin, P. Kim, H.L. Stormer, D.N. Basov, Dirac charge dynamics in graphene by infrared spectroscopy, Nat. Phys. 4 (2008) 532. http://dx.doi.org/10.1038/nphys989.